A Frequency Domain Model for evaluating Dynamic Compensator Response

P.H. Swart
School for Electrical and Electronic Engineering
Potchefstroom University, Private Bag X6001, 2531
Potchefstroom. phs@pop.onwe.co.za

Abstract – **Frequency-domain modelling of distorted voltage and current waveforms can be carried out for steady-state periodic behaviour by employing network analysis on a per-harmonic order basis and summing individual harmonic order results. When other requirements must also be met, such as the integration of system component design and the implementation of a new power theory, a "clean-sheet" approach is desirable, requiring the development of a new package, rather than the use of an existing commercially available one. This paper describes a frequency-domain model of the above nature that now forms the basis of a complete hybrid compensator design and modelling package development that is presently under way.**

Keywords: Harmonics, Compensation, Filters

I. INTRODUCTION

In hybrid compensation schemes for the mitigation of steady-state harmonics there are different configurations possible, employing a combination of line-commutated static-VAR compensators, passive filters and PWM-switched voltage-fed dynamic compensators (active filters) in series and in parallel with the supply. The series connections "insulate" the consumer from ambient system harmonics and the parallel ones aim at keeping the consumer's current harmonics out of the source[1]. Hybrid operation optimises the use of the different compensators, basically handing the bulk of the compensation to the low-cost passive filters and static-VAR compensators and using the dynamic compensators for controlled stabilisation and negative impedance injection. The ultimate hybrid compensator power- and control architecture has yet to be found and experimentation is continuing. The design and modelling of these alternative topologies is a cumbersome process and there appears to be a need for a single integrated package for accomplishing both tasks simultaneously. A beginning has been made with the development of such a package. It is not complete yet, but has been used so far in the modelling of an industrial plant with harmonic problems, for the installation of dynamic compensators. A design is carried out in which two PWM-controlled dynamic compensators are proposed and the design modelling without the compensators is verified by measurement.

II. POWER DEFINITIONS

Frequency-domain modelling is used. To cater for the needs of the analysis, the definitions of the IEEE Working Group on Non-sinusoidal Situations, under the chairmanship of A. Emanuel[2] has been selected and built into the model. Salient items belonging to these definitions that are used in the paper, are reviewed below for the convenience of the reader. Interested readers are referred to the literature for a more complete discussion.

The rms-scalar components of voltage U and current I can be separated into their fundamental and harmonic components:

$$U^2 = U_1^2 + U_H^2 \quad \text{and} \quad I^2 = I_1^2 + I_H^2 \qquad (1)\,(2)$$

with U_1 and I_1 the effective fundamental components of voltage and current and:

$$U_H = \sqrt{\sum_{n\neq 1} |U_n|^2} \quad \text{and} \quad I_H = \sqrt{\sum_{n\neq 1} |I_n|^2} \qquad (3)\,(4)$$

the corresponding effective harmonic components.

The *Total Apparent Power S* is defined as:

$$S = U I \qquad (5)$$

and the *Total Nonactive Power N* as:

$$N = \sqrt{S^2 - P^2} \qquad (6)$$

Alternatively, S can be defined as:

$$S^2 = (U_1 I_1)^2 + (U_1 I_H)^2 + (U_H I_1)^2 + (U_H I_H)^2 \qquad (7)$$

and grouped as:

$$S^2 = S_1^2 + S_N^2 \qquad (8)$$

in which S_1 is the *Fundamental Apparent Power* and S_N the *Nonfundamental Apparent Power*.
In turn:

$$S_1^2 = (U_1 I_1)^2 = (U_1 I_1 \cos\phi_1)^2 + (U_1 I_1 \sin\phi_1)^2 = P_1^2 + Q_1^2 \qquad (9)$$

and

$$S_N^2 = (U_1 I_H)^2 + (U_H I_1)^2 + (U_H I_H)^2 \qquad (10)$$

The term $(U_1 I_H)$ is named the *Current Distortion Power*, $(U_H I_1)$ the *Voltage Distortion Power* and $(U_H I_H)$ *the Harmonic Apparent Power*. The latter term can, in turn, be broken down into the *Total Harmonic Active Power* P_H and the *Total Harmonic Non-active Power* N_H.

$$S_H^2 = P_H^2 + N_H^2 \qquad (11)$$

in which N_H is derived analogously to N in (6).

Another useful relationship is obtained when (10) is divided by (9):

$$\left(\frac{S_N}{S_1}\right)^2 = \left(\frac{I_H}{I_1}\right)^2 + \left(\frac{U_H}{U_1}\right)^2 + \left(\frac{S_H}{S_1}\right)^2 \qquad (12)$$

to yield the *Normalised Non-fundamental Distortion Power*:

$$\left(\frac{S_N}{S_1}\right)^2 = (\text{ITHD})^2 + (\text{UTHD})^2 + (\text{UTHD}\cdot\text{ITHD})^2 \qquad (13)$$

The three RH-terms of (13) respectively represent the *current THD*, the *Voltage THD* and the product of the previous two. The significance, applicability and utility of the different components defined above are expounded in the literature[2].

The single-phase relationships of (1) and (2) are extended to unbalanced three-phase networks by the following definitions that lay down *the equivalent three-phase voltages and currents*:

$$U_e = \sqrt{\frac{U_a^2 + U_b^2 + U_c^2}{3}} \qquad (14)$$

and

$$I_e = \sqrt{\frac{I_a^2 + I_b^2 + I_c^2}{3}} \qquad (15)$$

The identical procedures used in (1) to (13), for single-phase values of voltage, current and power are also applicable to their *equivalent three-phase values* by replacing U and I respectively with U_e and I_e,. These equivalent values furnish a means of analogously handling three-phase data.

III. FREQUENCY-DOMAIN MODELLING

A. *Modelling approach*

Transient- and non-periodic system behaviour can only be modelled through numeric integration. This method becomes very slow in systems with a large number of nodes and has the further disadvantage of yielding limited analytical insight. In the case of systems operating under steady-state periodic conditions the frequency spectra are discrete and frequency-domain analysis can be adopted on a per-harmonic order basis, immunising it from the named disadvantages of network size and computation speed.

The approach used in frequency-domain modelling is to apply network analysis separately at each harmonic order in turn and then synthesise composite values of current, voltage and power[3]. It is at this last level that an acceptable power theory is essential.

The modelling approach here, calls for the multi-frequency modelling of transmission components like the supply authority source, cables, transformers and different types of periodic distortion loads such as controlled 6-, 12- or 24-pulse AC/DC converters. The elegance, versatility and user-friendliness of these models will probably contribute as much to the success of the model as all the rest and much care must be taken with them.

B. *Compound nodal circuit analysis*

The complex compound nodal network equation for harmonic order n, of an unbalanced three-phase power network with k nodes is written as:

$$[I(n)] = [Y_{bus}(n)]\,[U(n)] \qquad (16)$$

in which $[I(n)]$ and $[U(n)]$ are column vectors of dimension k.

$$\begin{bmatrix}[I_1(n)]\\ [I_2(n)]\\ \dots\\ [I_k(n)]\end{bmatrix} = \begin{bmatrix}[Y_{11}(n)][Y_{12}(n)]\dots[Y_{1k}(n)]\\ [Y_{21}(n)][Y_{22}(n)]\dots[Y_{2k}(n)]\\ \dots\quad\dots\quad\dots\quad\dots\\ [Y_{k1}(n)][Y_{k2}(n)]\dots[Y_{kk}(n)]\end{bmatrix}\begin{bmatrix}[U_1(n)]\\ [U_2(n)]\\ \dots\\ [U_k(n)]\end{bmatrix} \qquad (17)$$

The elements of $[I_j(n)]$ and $[U_j(n)]$ in which $j = 1,\dots,k$ are sub-vectors of dimension 3, defined respectively in terms of the line-currents and line-neutral voltages as:

$$[I_j(n)] = \begin{bmatrix} I_{ja}(n)\\ I_{jb}(n)\\ I_{jc}(n)\end{bmatrix} \quad \text{and} \quad [U_j(n)] = \begin{bmatrix} U_{ja}(n)\\ I_{jb}(n)\\ I_{jc}(n)\end{bmatrix} \qquad (18)(19)$$

$[Y_{bus}(n)]$ is a square $k \times k$ matrix and is termed *the n-th harmonic order nodal compound bus-admittance matrix.* The elements $[Y_{ij}(n)]$ of $[Y_{bus}(n)]$ in which $i,j = 1,\dots k$ represent compound admittances that are each square sub-matrices of dimension-3, defined as:

$$[Y_{ij}(n)] = \begin{bmatrix} Y_{ijaa}(n) & Y_{ijab}(n) & Y_{ijac}(n)\\ Y_{ijba}(n) & Y_{ijbb}(n) & Y_{ijbc}(n)\\ Y_{ijca}(n) & Y_{ijcb}(n) & Y_{ijcc}(n)\end{bmatrix} \qquad (20)$$

Sub-matrices (20) on the diagonal of $[Y_{bus}(n)]$ each individually defines an inter-node compound admittance and relates to the three phase values of that compound admittance. The diagonal elements of the sub-matrices (20) define driving-point compound admittances and the off-diagonal elements define the mutual compound admittances. Where mutual coupling exists between the three phases $[Y_{ij}(n)]$ as depicted by (20) will have non-zero off-diagonal elements. If all mutual coupling can be ignored, the compilation of $[Y_{bus}(n)]$ is a relatively simple task and can be carried out by inspection. Where mutual coupling does exist between different circuit sections, it is expedient to use the method developed by Arrilaga[4] in the compilation of $[Y_{bus}(n)]$.

In the modelling sub-vectors (18) and (19) are modelled in terms of their *harmonic phasor* values:

$$U_{jm} = U_{jm}(n)e^{j\alpha_{jm}(n)} \quad \text{and} \quad I_{jm}(n) = I_{jm}(n)e^{j\beta_{jm}(n)} \qquad (21)\,(22)$$

with $m = 1,2,3$.

The unbalanced vector node voltages $[U_{im}(n)]$ are presently obtained by analytically inverting $[Y_{bus}(n)]$ in (16) and solving separately for each harmonic order. With the unbalanced three-phase node voltages known for every harmonic order, corresponding branch currents and powers are easily calculated.

The analysis commences with the fundamental $n = 1$ and proceeds to the highest order, say the 45th as used in the present modelling. When the modelling is complete for every harmonic order, the results are summed for each node in accordance with (1) to (15).

When all mutual coupling is ignored, only the main diagonal sub-matrices (20) in $[Y_{bus}(n)]$, will have non-zero elements on their main diagonals which may be respectively modelled as:

$$Y_{ijlmL}(n) = \frac{1}{R_{ijlm}(n) + jn\omega L_{ijlm}} \qquad (23)$$

and

$$Y_{ijlmC}(n) = G_{ijlm}(n) + jn\omega C_{ijlm} \qquad (24)$$

for the series inductive and shunt capacitive elements of each of the three phases. In these equations, the harmonic order n merely scales the inductive-reactance and capacitive susceptance linearly and discretely for specified values of n.

C. Transmission-component models

Transmission-component models are embedded in the main model in the form of self-contained sub-models[1]. In this way, a quick change of models is possible and a library of models can be built up over time. The Mathcad-approach also furnishes a flexible and versatile "clean-sheet" approach to the user by means of which he can develop his own models from the grass-roots level.

The supply-authority source is modelled as a Norton-equivalent circuit for which the fundamental component admittance is calculated from the symmetric short-circuit fault-value.

Transformer sub-models are generated in accordance with the Arrilaga-approach[4], which consists of writing down the primitive admittance matrices and then converting for transformer configurations through connection-matrices.

The AC/DC 6-pulse converter modelling is carried out in a practical way. Physical line-current waveforms are matched in the model to actual measured profiles by adjusting the frequency-domain model parameters for firing-angle, peak current, sinusoidal pulse-width, conduction angle, fundamental phase and commutation angle[5]. The model synthesises the actual converter-bridge line-line currents from which the line-currents are calculated through Δ-Y transformation in the frequency-domain. In this way it is possible to cater for typical converter waveforms that range from converters with discontinuous DC-output currents to units with very large DC-chokes. This approach also has the advantage of eliminating zero-sequence current components. The same approach is used with 12- and 24-pulse units. The converter models are presently being extended to accept system parameters such as line- and choke inductances etc, which will be used for specifying new systems and in which measurements can not be used to obtain the initial current waveforms.

Passive filter sub-models are also embedded in the main model and the design-section is an integral part of the sub-model. Passive filter capacitors draw on the fundamental power factor requirement, but can be adjusted to shift resonance when required. Other aspects of passive filter design include selection of filter-arm configurations[4] and impedance-scans. The user specifies the amount of detuning and the required frequency deviation factor according to Kimbark[6], iteratively with each modelling exercise.

The dynamic filter models described in this paper are still relatively crude and make provision for PWM-controlled voltage- or current-fed topologies. In effect, the model now provides only for adjustment of the discrete frequency-response multipliers at the selected harmonic values. The data is stored in a look-up table in accordance with Table 1 and is compiled by matching the behaviour of the compensator model against observed performance.

Table 1. Compensator model response weighting

1	2	3	4	5	6	7	8	9	10
100	100	100	98	97	96	95	90	85	80
11	12	13	14	15	16	17	18	19	20
76	74	72	70	68	64	62	60	58	56

D. Modelling Procedure

Modelling is carried out through a manual-iterative procedure. Initially the sub-models are configured with all the known physical system-parameters as well as guesses for the others. During initial runs, the sub-model parameters are upgraded and tuned against physical measurements until the desired time-domain operating parameters and waveform matches are achieved. It is very important here for the user to thoroughly understand the physical system he is simulating, the model he is using and the relevant theory. Failing that, causes and effects are difficult to connect and fine-tuning becomes impossible.

If all the system-parameters were complete and correct, matching with the real system would not be necessary in the first place. Unfortunately there are very few systems in the real world for which complete parameter-data are available and this method of modelling then furnishes an additional very important inherent feature. *An accurately tuned model will furnish all the hidden and difficult to measure system parameters.* In the modelling described below, for example, the operation of the six-pulse converters is analysed, yielding several otherwise hidden characteristics. In addition, the accuracy of modelling of this type can be as high as the situation demands and include modelling results of sufficient accuracy to isolate active power flows of only a few watt hidden in harmonic frequencies in megawatt systems[7].

IV. VERIFYING THE MODEL

A. Circuit Description

It is doubtful if anyone anywhere will be prepared to furnish important modelling results before being able to tune a new model against measured results of one kind or another. Where extensions have to be made to existing systems, this is a relatively easy exercise. If new systems have to be modelled from the ground up, accurate system parameters are essential and it will be compared wherever possible with actual system or sub-system performance to improve the credentials of the model before laying one's head on a block. In the present case, an operating system was available to which dynamic compensation had to be added.

The diagram in Figure 1 represents the 11 kV busbars, with two 800 kVA 4.25% impedance Δ–Y step-down transformers that feed three plasma burner phase-controlled AC/DC converters. As shown, the bus-section between nodes 2 and 3 are kept open to achieve an acceptably low fault level. The 11 kV supply actually consists of a ring-feed, but it is convenient to model it here as a Thevenin equivalent source. The three burner loads are

1 Using the "Include" function in Mathcad.

shown as well as the provision for the two compensators F_1 and F_2. The rest of the diagram is self-explanatory.

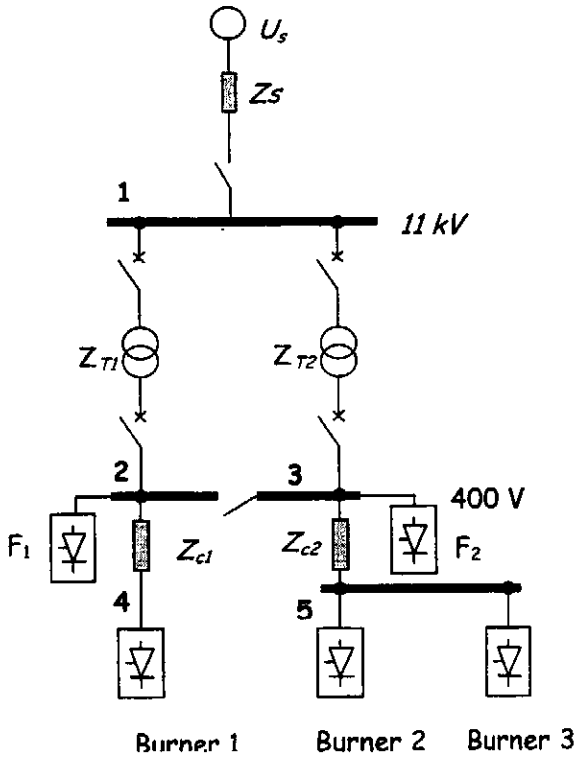

Figure 1. Power supply to burners

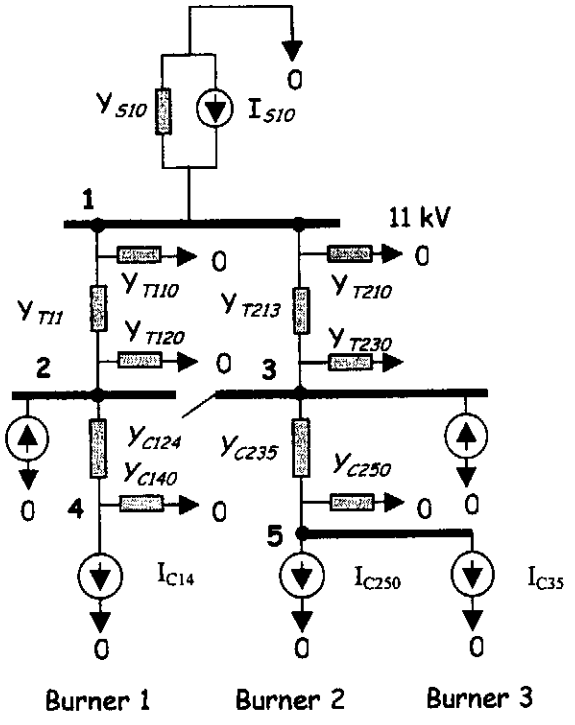

Figure 2 – Compound admittance diagram

The compound admittance diagram in Figure 2 is obtained by direct transformation of the single-line diagram in Figure 1. Nodes 1, 2 and 3 respectively represent the 11 kV busbars and sections 1 and 2 of the 380 V busbars. The transformers are modelled as π-models and the cables as L-models. Burners 1, 2 and 3 are modelled as current sources. Converter 1 is connected to node 4 and converters 2 and 3 to node 5.

B. Measurements for verifying the model

All three burners are operated at full power. The line-neutral voltage on node-2 and the low-voltage line-current on transformer 1 are recorded and are shown in the oscillogram in Figure 3. The vertical voltage scale is 100 V/div and that of the current is 200 A/div. The load current of burner 1 is seen to exhibit the characteristic 6-pulse phase-controlled current waveform for converters with large DC-choke inductance. This large inductance is inserted in the case of the burners to assist in maintaining the current during large burner resistance fluctuations. Note the dissimilarity in the magnitude of the two current-steps on either side of the peak-current step. This dissimilarity is present in both the positive going as well as in the negative-going current waveforms.

The notching in the voltage waveform is also clearly discernible. It is the presence of this notching that introduced the high frequency resonance with the fluorescent light fittings and the consequential overheating of circuit breaker trip-coils that drew attention to the presence of distortion in the first place. The secondary voltage of transformer 2 on node 3 also exhibits the same type of notching. Recordings of the transformer primary voltages shows hardly any notching and the immediate conclusion is that the transformer leakage impedances are the main culprits responsible for the trouble.

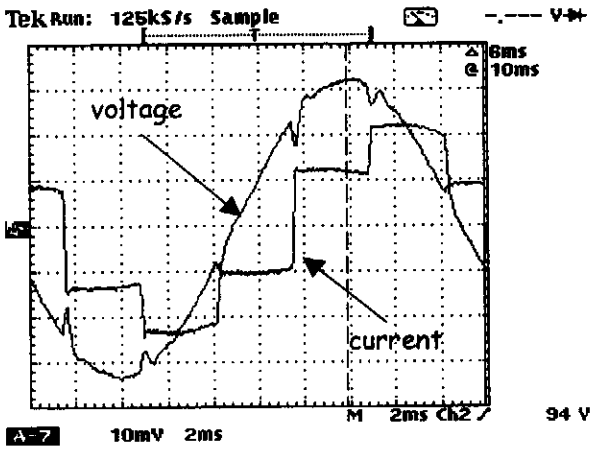

Figure 3. Measured voltage and current node-2

The voltage and current-data in Figure 3 is digitised and supplied to the model. It is then converted to frequency-domain data by means of a Discrete Fourier Transform (DFT) and back again to time-domain data by Inverse Fourier Transform (IFT). This, rather elaborate procedure of converting the steady-state periodical data to the frequency-domain gives it greater manoeuvrability. Firstly it is now possible to adjust the graph magnitude and time scales at will; a feature that comes in very handy during the comparison of measured and modelled data. The same measurement-results of Figure 3 are now repeated in Figure 4 but with expanded voltage and current scales and with a time-shifted waveform that now reflect two periods instead of 1. Another advantage of having the data in frequency-domain format is that it now becomes possible to

calculate powers and other data accurately, but also to transform synchronous three-phase data between phase and line values.

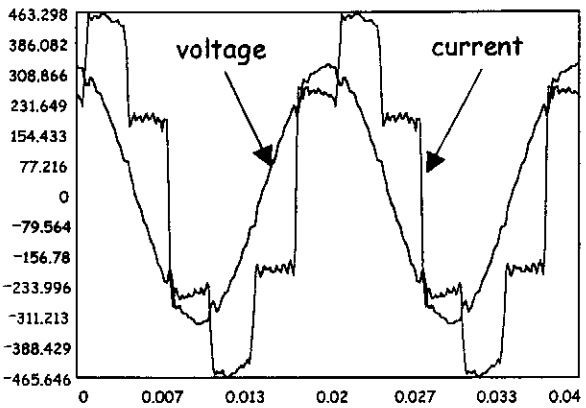

Figure 4. Time-domain reconstruction of measured voltage and current on node-2

After setting up the model and after some trimming, the results shown in Figure 5 is obtained.

C. Comparison of modelled results

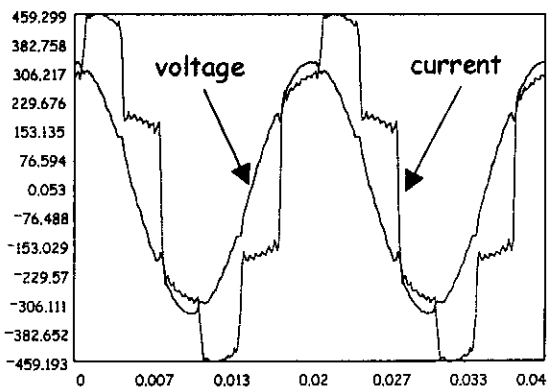

Figure 5. Time-domain modelling of voltage and current on node-2

The three phases are modelled separately throughout. It is therefore possible to separately adjust the individual phase firing angles and other controlling parameters on each converter and to also separately adjust individual phase voltages and even the individual phase admittances elsewhere in the model. In this way, the asymmetric current behaviour observed in Figure 3 and in Figure 4 can be matched. A match was obtained in this instance with the physically recorded waveforms by adjusting the peak bridge converter currents and firing angles.

The modelled and measured frequency-domain data is compared in Table 2. Unless otherwise specified, all voltages and currents are in rms-values. The accuracy of the modelling can be verified here. It must be noted that it does take an amount of effort to tune model parameters until an acceptable match is obtained and that the effort is exponentially related to the final accuracy that is required. This is so, because great accuracy can only be obtained when all the component parameters match and when, in the end, parasitics and mutual couplings are also included. The information in Table 2 utilises the IEEE Working-Group single-phase definitions that have been defined in (1) to (13) and displays the phase-a values.

Table 2. Modelled against measured results

Description	Modelled	Recorded
Voltage Node:	2	2
Start Current Node:	2	2
End Current Node:	4	4
Node Voltage	231.734	227.4
Fundamental Voltage(V):	231.486	227.1325
Harmonic Voltage(V):	10.7174	11.0263
Node-node Current(A):	311.9664	313.285
Fundamental Current(A):	303.1014	300.7829
Harmonic Current(A):	73.8412	87.6192
Apparent Power(kVA):	216.8796	213.723
Non-active Power(kVA):	153.6933	150.9863
Fundam. Appar. Power(kVA):	208.55	204.95
Current Distort. Power(kVA):	51.2796	59.7035
Voltage Distort. Power(kVA):	9.7454	9.9495
Joint Harm. Power(VA):	2.254.26	1926.07
Harmon. Appar. Power(kVA):	2.3742	2.8983
Current THD(%):	24.3619	29.1304
Voltage THD(%):	4.6298	4.8546
Norm. Har. Appar. Power(%):	1.1279	1.4142
Displacement Power Factor:	0.7338	0.7413
Overall Power Factor:	0.7056	0.7078

V. MODELLING WITH DYNAMIC COMPENSATORS INSTALLED

Two 150 kVA, IGBT-switched, PWM-controlled, three-phase dynamic compensators were on hand and an investigation was necessary to determine if their installation on the low-voltage busbars would solve the harmonics problem. It was possible to characterise the frequency-response of the two identical compensators through a modelling comparison with this same package where they were used in a previous installation and to compile the frequency-response weighting factors depicted in Table 1 during that exercise. It must be mentioned here that these compensators employ a simple steady-state control scheme by means of which the measured distorted load current is generated by the compensator and injected at the point of common coupling. This control system permits the fundamental and harmonic components to be collectively or separately compensated so that the required magnitude of the one can be traded off against that of the other if the need arises.

Analysis by means of the model showed that compensator 1, which was required to compensate a single burner, could compensate for both the fundamental power factor and for the harmonics. Compensator 2, however, had to be adjusted to compensate for the harmonics only on account of the higher load. The modelling is therefore based on that recommendation. Because of the relatively high leakage reactance of the transformers, each LV section now has to contend with its own harmonics and the voltage distortion on the LV side.

Modelling results for the compensator phase-a line-neutral voltages and line-currents are shown in Figure 6 and Figure 7. Note that there is a fundamental component of current present in the first, which lacks in the second.

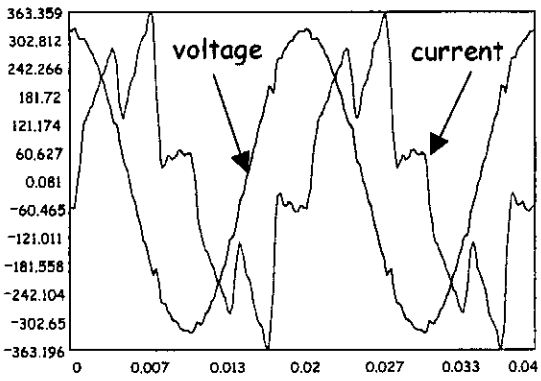

Figure 6. Compensator 1 current and node 2 voltage

Notice also that there are perceptible improvements in the voltage traces on node 2, when compared with the previous results, without compensation as depicted in Figure 5.

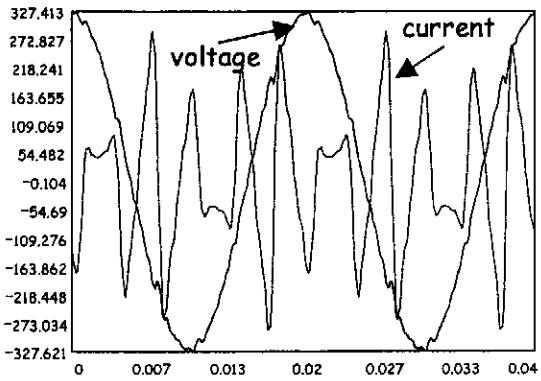

Figure 7 – Compensator 2 current and node 3 voltage

The compensator performance is best illustrated in tabular form as in Table 3 and is analysed in terms of the IEEE Working-group definitions defined in (1) to (13).

Table 3 – Operating data for the compensators

PARAMETER	COM 1	COM 2
Node Voltage(V)	226.944	226.94
Fundamental Voltage(V)	226.8533	226.85
Harmonic Voltage(V)	6.427	6.427
Current(A)	219.78	131.212
Fundamental Current(A)	209.9306	0
Harmonic Current(A)	65.0688	131.212
Apparent Power(kVA)	141.6359	89.3337
Non-active Power(kVA)	149.6056	89.3337
Fund. Apparent. Power(kVA)	141.49	0
Current Distort. Power(kVA)	44.2832	89.2979
Voltage Distort. Power(kVA)	4.0477	0
Harm. Apparent Power(kVA)	1.2546	2.5299
Voltage THD(%)	2.8331	2.8331
Displacement Power Factor:	0.0213	0

Note the absence of a fundamental current in the case of compensator 2. It is also interesting to note that the harmonic voltage and the fundamental voltage for compensator 1 are orthogonal and must be added as $\sqrt{6.427^2 + 226.8533^2}$ to obtain the node voltage. This is also true for the compensator current in which the addition must be carried out as $\sqrt{65.0688^2 + 209.9306^2}$. Also note that the displacement power factor is virtually zero for both compensators, confirming that these units only supply non-active power. The voltage distortion is also seen to reduce on node-2 from 4.629% down to 2.833% with dynamic compensation.

VI. CONCLUSIONS AND RECOMMENDATIONS

The model accuracy is proven in comparing modelled-with measured results on node-2. The verified model is then considered accurate enough to be used in analysing the performance of the dynamic compensators. In the interest of this paper, results depicted here is used to emphasise the modelling virtues rather than the improvement in the system harmonic conditions. That has been done in other analyses, but falls beyond the scope of this paper. The modelled results for the performance of the compensators are credible and realistic and can be proven by adding the compensator current to the load currents. That has not been done here as well to conserve space.

It will only be possible to assess the measured performance of the compensators against the modelled waveforms when the compensators are commissioned later.

VII. ACKNOWLEDGEMENT

The Atomic Energy Corporation of SA is acknowledged for their permission to publish the paper.

LITERATURE REFERENCES

[1] N. Balbo et al., "Simplified Hybrid Active Filters for Harmonic compensation in low voltage Industrial Applications", *Proceedings of ICHPS VI*, pp. 263-269, 1994, Bologna Spain.

[2] IEEE Working group on Non-sinusoidal situations, "Practical Definitions for Powers in Systems with Nonsinusoidal Waveforms and Unbalanced Loads: A discussion", *IEEE Trans. On Power Delivery*, Vol. 11, January 1996.

[3] J.H.C. Pretorius, N.J. Truter, P.H. Swart, J.D. van Wyk, "Power-line conditioning of a multi-kilowatt laser plant", *Proceedings of the. IEEE 4th Africon conference in Africa*, Stellenbosch, South-Africa, Sept. 1996, pp. 810-815.

[4] J. Arrilaga, C.P. Arnold, B.J. Baker, *Computer Modelling of Electrical Power Systems*, John Wiley & Sons, New York, 1983.

[5] D.E. Rice, "A Detailed Analysis of Six-Pulse Converter Harmonic Currents", *Proceedings of the IEEE Transactions on Industry Applications*, Vol. 30, No. 2, March 1994, pp 294-304.

[6] E.W. Kimbark,. *Direct Current Transmission*, John Wiley, New York, 1971.

[7] P.H. Swart, M.J. Case, J.D. van Wyk, "On Techniques for Localisation of Sources Producing Distortion in Three-Phase Networks", European Transactions on Electrical Power Engineering (ETEP), Vol. 6. No. 6, Nov/Dec 1996.